Available at www.ComputerScienceWeb.com
POWERED BY SCIENCE DIRECT®

Pattern Recognition Letters 24 (2003) 1971–1982

Pattern Recognition Letters

www.elsevier.com/locate/patrec

Analysis methods of CT-scan images for the characterization of the bone texture: First results

A. Taleb-Ahmed [a,*], P. Dubois [b], E. Duquenoy [a]

[a] *Laboratoire d'Analyse des Systèmes du, Littoral Cote d'Opale, BP 649, Calais 62228, France*
[b] *Institut de Technologie Médicale, Centre Hospitalier et Régional de Lille, Lille 59000, France*

Received 30 April 2002; received in revised form 10 February 2003

Abstract

The ultimate objective of the planned work is to propose a way to the characterization of the bone texture from the analysis of CT-scan images. This would assist the discrimination of healthy from pathological subjects. This paper emphasizes a preliminary study concerning the selection of tools for the characterization of the bone texture. The selectivity is lead by the analysis of respective sensitivities of the considered methods. We study here two methods of texture analysis. The first one is based on the fractal geometry whose application to the analysis of texture is well established in literature. The second method is an original one. It is called the "method of the three dimensional relief".

Keywords: Characterization of the bone texture; Fractal method; Three dimensional relief; CT-scan images

1. Introduction

Osteoporosis is a bone pathology inducing an increased fragility of the skeleton. It appears more frequently to women for hormonal reasons (menopause). It is also linked to the advancing age: indeed, at the age of 70, the density of the skeleton has decreased by 1/3. With the lengthening of the duration of life, this pathology is going to concern an increasing population. It often entails fractures of the wrist and the femur neck (55 000 fractures per year in France, which cause death in 25% of the cases).

The early diagnosis of osteoporosis leads to a better medical treatment. Among the means currently available in routine clinic, the medical imaging brings privileged means of detection. A good knowledge of the bone structure allows a better prevention of the risks of bone fracture. Indeed, a healthy person owns large and long bone frameworks which characterize the quality of the bone structure. At the opposite, the patient affected by bone pathology shows an altered fractured bone structure. Among currently proposed methods, the bone biopsy remains traumatic and therefore is rarely practiced.

* Corresponding author. Tel.: +33-321465654; fax: +33-321460683.
E-mail addresses: taleb@lasl-gw.univ-littoral.fr, abdelmalik.taleb-ahmed@lasl-gw.univ-littoral.fr (A. Taleb-Ahmed).

0167-8655/03/$ - see front matter
doi:10.1016/S0167-8655(03)00036-9

The ultimate purpose of the planned work is to give the means of characterizing the bone texture from the analysis of CT-scan images. This would assist the discrimination of healthy from pathological subjects. One of the constraints is to find methods of analysis independent of the operator. In that purpose we want to develop reproducible solutions, inter and intra operator. This paper emphasizes a preliminary study concerning the selection of some characterization tools of the bone texture. There are generally three classes of analysis related to the texture characterization in images: (i) statistical, (ii) structural and (iii) fractal analysis.

Statistical parameters account for local properties of the image. Structural parameters inform on both the physical limits of the objects framing the image and the homogeneity of the surface of these objects. Finally the fractal geometry gives a measurement of the complexity and the global irregularity of the bone texture.

1.1. Brief overview of texture analysis

A distinction may be made between two approaches for texture analysis: the statistical approach and the structural one. In statistical approaches, texture is quantified on the basis of the (local) spatial distribution of the gray-values parameters (Benhamou and Lespessailles, 1994; Benhamou and Harba, 1994; Lynch and Hawkes, 1991; Jin and Ong, 1995; Pothuaurd and Lespessailles, 1998; Osman and Newitt, 1998).

In structural techniques, the image is described in terms of textural elements and their spatial relationships. Most of the texture-analysis algorithms described in literature have been used to classify quite dissimilar textures. Since the visually perceived differences in bone texture in radiographs are subtle, the texture-analysis method has to be rather sensitive. Various statistical methods of texture analysis were applied in order to translate the differences of bone structure into a set of information easily exploited. Current research is focused on morphological texture parameters and on comparing the usefulness of the different techniques in distinguishing patients with clinical osteoporosis from their healthy contemporaries (Serra, 1982; Cuisenaire, 1999; Vieth, 2000; Muller and Hahn, 1996).

In the present study, we investigated the value of bone texture analysis from CT-scans of the distal radius, obtained with a conventional machine.

We study here two methods of texture analysis. The first one is based on the fractal geometry whose application to the analysis of texture is well established in literature. After a brief review of fractal geometry in Section 3, we examine two methods for the estimation of the fractal dimension: the method of variations and the method of morphological covering. We provide details of their implementation and list the results obtained from their application on synthetic and real images. In Section 4, an original method for the analysis of bone texture, called the "method of the three-dimensional relief", is presented. It is related to the structural analysis and is based on the study of primitives. After a general description of this method, we present the tools used in the different processing steps and its implementation on CT-scan images. We provide details of their implementation and list the results obtained from their application on real images. Finally, in Section 5 the conclusion and the prospects are listed.

2. Materials and method

2.1. Materials

CT-scans were undertaken on an Elite Plus™ with a high-resolution algorithm. For each patient, four consecutive axial and four consecutive coronal slices of the nondominant forearm were selected. The first axial slice was performed just above the rest of the epiphyseal cartilage and the first coronal slice was located on the anterior part of the distal radius (Fig. 1).

To avoid artifacts on coronal slices, there was an angle of 22° between the main axis of the radius and the hand. The following CT settings were used: slice thickness 1 mm; field of view 140 mm; pixel matrix 512×512; pixel size $\approx$200 μm leading to a maximum spatial resolution of $\approx$400 μm. Each pixel is coded on 12 bits or 8 bits. The size of

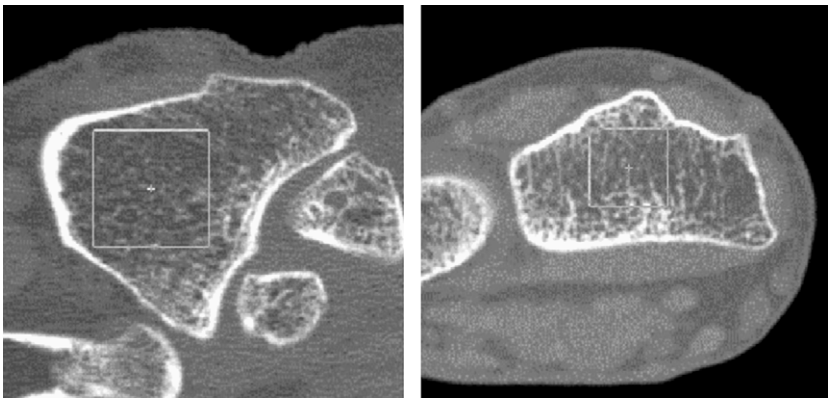

Fig. 1. Coronal (left) and axial (right) slices.

the region of interest (ROI) was adjusted to the size of the image (from 8×8 mm^2 to 17.4×17.4 mm^2). The choice of the ROI is carried out according to the following criteria:

- Its shape is square.
- Its size is variable (the largest possible to improve the statistical calculation).
- Its position is variable according to the user.
- The ROI must always exclude the cortical bone.
- The ROI is selected by a doctor.

Images were transferred to a PC computer and two kinds of bone texture analysis were carried out: fractal analysis and structural analysis. The algorithms used to characterize the bone texture were all developed in the laboratory of Calais and the laboratory of Biophysics of the University Hospital of Lille.

2.2. Subjects

Patients were selected in the department of Rheumatology of the University Hospital of Lille. Two distinct studies were carried out. Each study was carried out on groups of 30 women:

In the first study, 30 postmenopausal women were studied. According to their bone status they were divided into two groups. Group I consisted of 15 postmenopausal osteoporotic women without disease affecting bone mass or bone metabolism. Group II was composed of 15 controls women. Neither the patients nor the controls were receiving treatment affecting bone mass or bone metabolism. Eight slices were selected on each patient: four consecutive coronal slices and four consecutive axial slices. Bone texture analysis was performed using the method of morphological covers leading to the measurement of two features (D_f and S_f). The ages of the postmenopausal osteoporotic women and controls were not statistically significantly different: 68 ± 10 years versus 66 ± 9 years ($p = 0.4$). Although both mean weight and mean height were higher in controls compared with the osteoporotic women the difference did not achieve significance: 69 ± 16 kg versus 65 ± 14 kg ($p < 0.3$) and 161 ± 7 cm versus 157 ± 6 cm ($p < 0.06$), respectively.

In the second one, another group of thirty women was studied. According to their bone status they were divided into three groups. Group I consisted of 8 postmenopausal women without disease affecting bone mass or bone metabolism. Group II consisted of 7 women suffering from postmenopausal osteoporosis. Group III consisted of 15 control women before menopausal. Eight slices were selected on each patient under the same conditions as the previous groups: four consecutive coronal slices and four consecutive axial slices. Bone texture analysis was carried out with structural analysis leading to the measurement of five features:

- crest length/ROI,
- average size of the large valleys/ROI,
- number of large valleys/ROI,

- average size of the small valleys/ROI,
- number of small valleys/ROI.

The age of the controls women (group III) before menopausal is 33.1 ± 10.6 years and the ages of postmenopausal osteoporotic women and postmenopausal women (groups II and I) were statistically significant: 67 ± 9 years ($p < 0.01$).

Some comparisons between the bone texture variables in osteoporotic patients and control patients were performed by using the nonparametric Mann–Whitney U-test due to the low number of patients in each group. A value of $p < 0.05$ was considered as statistically significant. The results are expressed as mean $\pm$ standard deviation.

3. Fractals

The bone structure is relatively good for fractal geometry because of its complicated and irregular character. The fractal analysis is used for the bone structure analysis because the estimated value of fractal dimension is real. This fractal dimension varies with the structure alteration of the trabecular bone and thus with the thinning of the trabecular network due for example to osteoporosis. The fractal dimension is given by:

$$D_{\mathrm{f}} = -\frac{\log(n(\varepsilon))}{\log \varepsilon} \tag{1}$$

where $N(\varepsilon)$ represents a size (surface, volume,...) characterizing the object when searching for its fractal dimension. ε represents the resolution with which the size is calculated. Hausdorff (1919) and Minkowski (1901) presented the fractal dimension of the object at the beginning of the 20th century.

3.1. The methods for estimating the fractal dimension

As seen before, the fractal dimension estimation lays on the parameter variation characterization, like the perimeter, the surface or the volume; it depends on the size of the covering element. There are a lot of methods for fractal analysis like the methods of the boxes, the method of variations and the morphological covering method. For these methods, the fractal analysis considers the image as a three-dimensional distribution. Indeed, three components are taken into account: the location of the pixel in the image (x, y) and its gray level value (z). The method of boxes, although easily set up, has a major drawback which is the error rate of the fractal dimension. In fact, during the volume description by a structuring element (an ε sized cube), the occupation rate of this structuring element on the curve is not taken into account (Prasad and Majunbar, 1991).

3.2. Method of variations

This method allows us to determine the fractal dimension according to Minkowski. In (Vieth, 2000), this method was applied to the estimation of the fractal dimension of a curve. We achieved an extension of this method in order to adapt it to the characterization of our surface. Like Minkowski's definition given previously, this method searches to define the covering case. In our situation the initial object is a surface, our case will then be a volume one. This case will be determined from the maximum variation of the gray-levels, upon a window (size ε), for every surface point. The window will have to be moved on the whole S surface. The maximum variations are represented by the extreme values of the gray-level, in fact the minimum and maximum are located on the same window. This variation will change according to the dispersion of the gray-levels. The larger the size of the structuring element will be, the higher the range of maximum values of gray levels we get.

3.2.1. Application of the method

Let T be the side value of our square picture I, each pixel of this picture will be referenced by its co-ordinates (i, j). For each of these points, we are going to determine the maximum and the minimum value of the gray-level upon the neighbourhood selected by the window (sized ε). We obtain:

$$\mathrm{Max\_wind}_{\varepsilon}(x, y) = \max_{\substack{x-\varepsilon/2 \leqslant i \leqslant x+\varepsilon/2 \\ y-\varepsilon/2 \leqslant j \leqslant y+\varepsilon/2}} I(i, j) \tag{2}$$

where the couple (x, y) represents the co-ordinates of the windows center. In a same way we define:

$$\text{Min\_wind}_\varepsilon(x,y) = \min_{\substack{x-\varepsilon/2 \leqslant i \leqslant x+\varepsilon/2 \\ y-\varepsilon/2 \leqslant j \leqslant y+\varepsilon/2}} I(i,j) \tag{3}$$

After obtaining the set of the minimum and maximum values for our picture, we can calculate the volume case G_V:

$$G\_V(\varepsilon) = \sum_x \sum_y \text{Max\_wind}(x,y) - \text{Min\_wind}(x,y) \tag{4}$$

So we calculate the volume cases for different sizes of the window, these windows are always applied to the original picture and not in a recursive way. However, the convolution between a T size square picture and an ε size window gives us a resulting square picture of this size:

$$T - 2 \times \text{integer}(\varepsilon/2) \tag{5}$$

The size of the resulting picture depends on our ε window size. For two different windows which are respectively the sizes ε and ε', the resulting picture will not have the same dimension. This difference of dimension will generate a graphical representation of volume cases in function of the ε size, which will be nonlinear. In this process, we must keep the picture size constant. In this purpose, we arbitrarily decided to stop the calculation of the volume case for a maximum window size equal to half the size of the original picture. We obtain the cases calculated by $\varepsilon = 3$ at $\varepsilon = T/2$. The set of values of the volume cases value gives us the curve:

$$\log G\_V(\varepsilon) = f(\log \varepsilon) \tag{6}$$

To reach the fractal dimension, we calculate the linear regression of this curve. We then obtain the slope, which will be noted:

$$\left[\frac{\log G\_V(\varepsilon)}{\log \varepsilon}\right]' \tag{7}$$

The fractal dimension is determined as follows:

$$D_f = 3 - \left[\frac{\log G\_V(\varepsilon)}{\log \varepsilon}\right]' \tag{8}$$

In this equation, constant 3 is due to the calculation of the fractal dimension by the volume (topologic dimension equal 3). We define another parameter, which is the fractal signature. The fractal signature represents the average of the local slopes, that is to say the slope between two consecutive values ε. We have then:

$$\text{local\_slope} = \frac{\log V(\varepsilon) - \log V(\varepsilon - 2)}{\log \varepsilon - \log(\varepsilon - 2)} \tag{9}$$

$$\text{Sign\_f} = 3 - \text{average}(\text{local\_slope}) \tag{10}$$

3.3. Method of the morphological covers

Peleg (1984) suggested this method. It consists in the calculation of the area covering the surface to be characterized. In order to determine the covering surface, we must define a lower surface and an upper surface. Both surfaces make then a covering of the original surface. gray-level erosion and dilatation of the original picture respectively determine the lower and upper surfaces. The differences (between the erosion and dilation) are summed on each pixel. It will give volume $V(\varepsilon)$ covering the surface of the picture. Let D_ε and E_ε be the results of the dilatation and erosion of the central point (i,j) of the window convolution with ε size, we have:

$$V(\varepsilon) = \sum_i \sum_j (D_\varepsilon(i,j) - E_\varepsilon(i,j)) \tag{11}$$

In this volume we're going to look for a surface. In order to obtain the covering area of this surface, we calculate the differential volume $\mathrm{d}V(\varepsilon)$. We then obtain:

$$A(\varepsilon) = \frac{\mathrm{d}V(\varepsilon)}{\mathrm{d}\varepsilon} \tag{12}$$

Just like with the previous method, the differential volume $\mathrm{d}V(\varepsilon)$ must be computed on a picture of constant size. We then obtain the following expression:

$$A(\varepsilon) = \frac{V(\varepsilon_a) - V(\varepsilon_p)}{\mathrm{d}\varepsilon}, \text{ where } \varepsilon_a > \varepsilon_p \tag{13}$$

As the size of the window must be odd, the variation of ε between the two successive windows will be equal to 2:

$$A(\varepsilon) = \frac{V(\varepsilon) - V(\varepsilon - 2)}{2} \tag{14}$$

We obtain, with if we use the definition of the fractal dimension given by Minkowski:

$$D_f = 2 - \left[\frac{\log A(\varepsilon)}{\log \varepsilon}\right] \quad (15)$$

Where $[\log A(\varepsilon)/\log \varepsilon]$ represents the slope of

$\log A(\varepsilon) = f(\log \varepsilon)$

In the same way as the variation method, we define the fractal signature given by:

$$\text{Local\_slope} = \frac{\log A(\varepsilon) - \log A(\varepsilon - 2)}{\log(\varepsilon) - \log(\varepsilon - 2)} \quad (16)$$

$$\text{and Sign\_f} = 2 - \text{average(local\_slope)} \quad (17)$$

Lynch and Hawkes (1991) showed that the best results are obtained by the use of a vertical or a horizontal window. After presenting the different methods of the calculation, we are going to see their application in the environment of the subject.

3.4. Application on synthetic pictures

To validate the results, we had to generate some fractal pictures with a known dimension. In order to generate some fractals, Mandelbrot introduced the Fractional Brownian Motion (FBM) (Mandelbrot, 1975). This FBM introduces another parameter H which is related to the fractal dimension as follows:

$$D_f = D_t + 1 - H \quad (18)$$

with D_f fractal dimension, and D_t topological dimension.

The H variable taking its values in the interval $[0, 1]$. From the relation (18) we find a dimension superior or equal to the topological dimension. We used the Saupe algorithm (Saupe, 1988). It involves the search of the middle point of the two points coming from a function, in a recursive way. This algorithm provides only an approximation of the FBM. An example of fractal image is shown in Fig. 2.

By varying the H parameter, we can obtain a set of synthetic images with fractal dimension in the interval $[2, 3]$. The dimension of the generated pictures are 2.001, 2.1, 2.2, 2.3, 2.4, 2.5, 2.6, 2.7, 2.8, 2.9 and 2.999, that is to say 11 various dimensions.

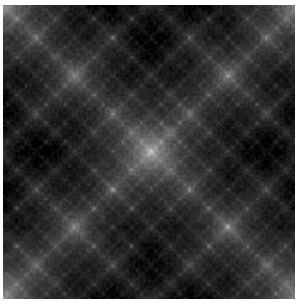

Fig. 2. Synthetic fractal image with $D_f = 2.5$.

4. Results and discussion

The method of variations provides estimations of the fractal dimension between 2.188 and 2.76 (Fig. 3). Consequently, it reduces the expected range of the fractal dimension (between 2 and 3).

The method of morphological covering produces a more extensive variation of the fractal dimension $[2.25, 3.23]$. However it delivers systematically overestimated results (Fig. 4).

If we want to choose between the two previous method, we have to consider both the method and the parameters which deliver the best sensitivity.

According to the two previous figures, the method of morphological covers shows the best range of variation, for the fractal dimension as well as for the fractal signature.

We thus proposed to study why we obtained with the method of the morphological covers some

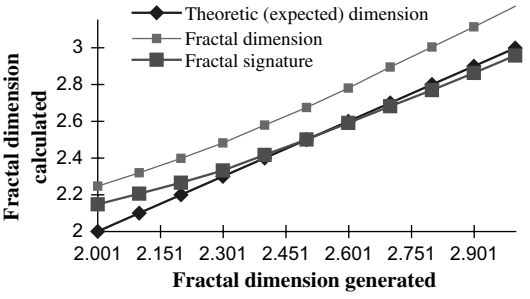

Fig. 3. Fractal dimension by the method of variation.

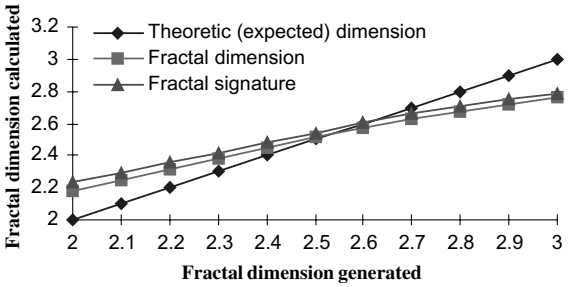

Fig. 4. Fractal dimension by morphological covering.

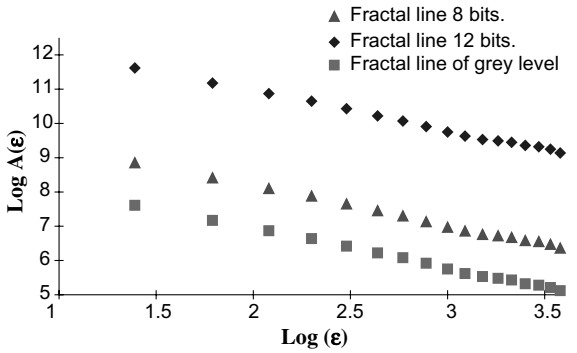

Fig. 5. Influence of dynamics on fractal dimension.

values which were higher than the theoretical dimension. We initially directed our study towards the influence of the number of gray-levels of an image on fractal dimension.

To carry out this study we used several images coded with 4 and 8 truncated bits and 12 original bits, we then plotted the curve $\log A(\varepsilon) = f(\log(\varepsilon))$ (Fig. 5). We can note that, for the three different dynamics, the lines are parallel and thus have identical slopes. Consequently, fractal dimensions will be equal. We can conclude that the number of gray levels is not the cause of an over estimate of the fractal dimension. An explanation could undoubtedly be given by multi fractal approach.

4.1. Application on real CT-scan images

To give a brief summary of our work, a priori and a posteriori, show that the fractal analysis seems notably effective in terms of discrimination between osteoporosis women and controls (Table 1).

Table 1
Bone texture fractal analysis between group I and group II on axial slices

Variables	Group I	Group II	p
Number	15	15	
Age	68 ± 10	66 ± 9	0.4
Years since menopause	19 ± 11	19 ± 11	Not significant
Weight (kg)	65 ± 14	69 ± 16	Not significant
Height (cm)	157 ± 61	61 ± 7	0.06
Sign_f	2.8 ± 0.17	2.69 ± 0.13	0.017
D_f	2.91 ± 0.15	2.72 ± 0.15	0.02

For the fractal analysis, the most promising structure parameters for CT images are fractal dimension, fractal signature (i.e., with the method of morphological covers). Indeed, some authors have shown that the fractal dimension measured on calcaneus or lumbar spine radiographs was significantly different in osteoroporotic women and in age matched controls (Buckland-Wright and Lynch, 1994; Benhamou and Lespessailles, 1994; Benhamou and Harba, 1994; Cortet and Dubois, 1998). But others did not note it (Lespessilles and Eynard, 1996). The noted differences could result from the mode of calculation of the fractal dimension. Indeed, in the work of (Lespessilles and Eynard, 1996), the fractal analysis was carried out by using the estimator of the maximum of probability according to the model of the fractional Brownian movement. Whereas in our study the fractal dimension was determined by the method of the variation and the morphological covers.

Nevertheless the results with fractal analysis are conflicting. (Majunbar and Genant, 1997; Majunbar and Link, 1999; Cortet et al., 2000) showed on MRI images that the fractal dimension was not statistically different in osteoroporotic patients and in controls after adjustment for age. However, we cannot exclude the possibility that the use of another method to calculate the fractal dimension could provide better results in terms of discrimination between osteroporotic and controls in MRI images.

This is why we studied and developed another approach. We will present a method based on the

approach of the structural analysis of texture: the three-dimensional relief method.

5. Three dimensional relief

As seen below, this method uses a structural analysis of the texture. The structural analysis gives a description of textures by studying the primitives that compose them. There are two methods to study these primitives. The first one is based on a description of the layout and the organization of the primitives. It is often used for strongly structured textures. In our case, our images relate to natural textures and are not therefore matched to this method. The second method is the three-dimensional relief. It is a description of the primitives and runs in two steps: the extraction of the primitives uses classical segmentation techniques such as thresholding or edge detection. A binarization is then made so as to characterize the obtained shapes more easily.

5.1. Description of the method

The image is considered as a relief being constituted by gray-level valleys and crests. On CT-scan images, the bone frameworks correspond to the clearest areas (highest gray-levels), the soft tissues of the trabecular bone correspond to the darkest areas. We will then get a mountainous relief where major values of gray-levels represent the highest altitudes, and low gray-levels will have the lowest altitudes. The aim of this method is to characterize the components of this relief, that it to say the crests and the valleys. This characterization is made by the means of a gray-level skeletonizing (Serra, 1982; Taleb-Ahmed et al., 2000). This skeletonizing outlines the valleys by the crests corresponding to the bone frameworks. Each valley gets a unique altitude and is therefore changed into a flat basin. The sides of each mountain form this basin and we associate the value of gray-level of the lowest point of the valley to the basin (Fig. 6). This lowest point can be compared with the running point of the rainwater into a valley.

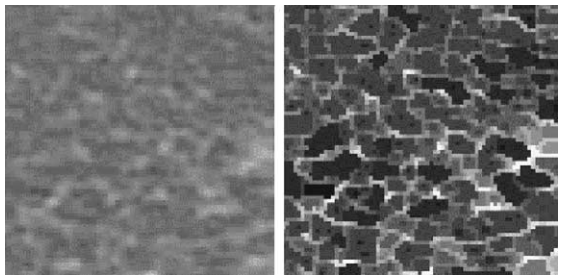

Fig. 6. ROI in coronal slice (left) and 3D ROI in coronal (right).

Crests formed by the tops of the «mountains» then delimit each basin. These crests form the watershed.

5.2. Implementation

As mentioned above, the first step of the method involves the extraction of the primitives with the help of a gray-level skeletonizing.

5.2.1. Gray-level skeletonizing

The skeletonizing is obtained after calculating successively two kinds of filters (Taleb-Ahmed et al., 2000). Thanks to this method, we obtain maxima gray-level that remains unchanged and that form the crests of the three-dimensional image. The flanks get the minimal value of the valley. The convolution of an image by a filter produces a consequent image smaller than the initial image. Considering the very large number of convolutions, we have to keep the image size constant. To achieve this result, we replicated the edges of the resultant image, so as to adjust the size of the image after each convolution. We checked that this operation had no or little impact on the final result. A trimming of the skeleton follows the skeletonizing.

5.2.2. Trimming of the skeleton

The trimming consists of the successive running of filters (Taleb-Ahmed et al., 2000) to suppress the artifacts induced by the skeletonizing. We can make two kinds (coarse and fine) of trimming. We then get the skeleton as illustrated by the Fig. 7 left.

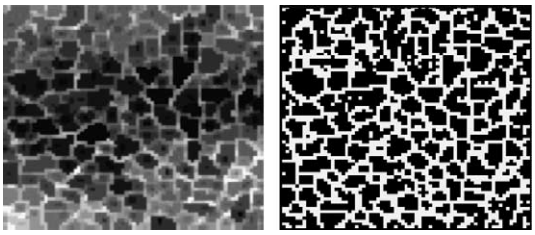

Fig. 7. Result of thinning after trimming and shaping of the crest line (right).

So, to extract the crests, we make the difference between the trimmed skeleton and the opened skeleton. The result is then binarized and gives a characterization of the shapes, as shown on the Fig. 7 right. We define from this binary image a characteristic attribute: the total crest length measured by the number of white pixels referred to the surface of the RIO.

5.2.3. Contour extraction

Then by inverting the binary image, we characterize the average valley surface by computing the number of the valleys constituting the image. Some errors in digitizing or processing the images can induce the generation of small illicit valleys, making then the number of the small valleys poorly representative. This is why we define an arbitrary threshold of surface rejection of these valleys. We obtain then two values: the average size of the small valleys and the average size of the large valleys, both referring to the surface of the ROI.

5.3. Evaluation and discussion

The tuning of this method was investigated in two ways: the determination of the thresholds for the rejection of the small valleys and the influence of the gray-level coding of the original dynamics.

5.3.1. Influence of the small valleys

So to eliminate the meaningless valleys, we search for an optimal rejection threshold of small valleys. The histogram of the valley sizes (Fig. 8) was computed for patients belonging to different groups: control patients (patient no. 1), bone pathologies (patients no. 2 and 3).

As we can see it, this histogram outlines a large recovering of the values and does not allow to select a rejection threshold. Consequently, we finally chose an arbitrary threshold of 4 pixels.

5.3.2. Influence of the gray-level coding

We studied a same image with different coding of the dynamics: 12 original bits and truncated 4 and 8 bits. The display (Figs. 9–11) of the obtained results with the same trimming process shows major differences.

The most appropriate dynamics to our study is the one which gave us the best discrimination and therefore offered the widest range of variation of

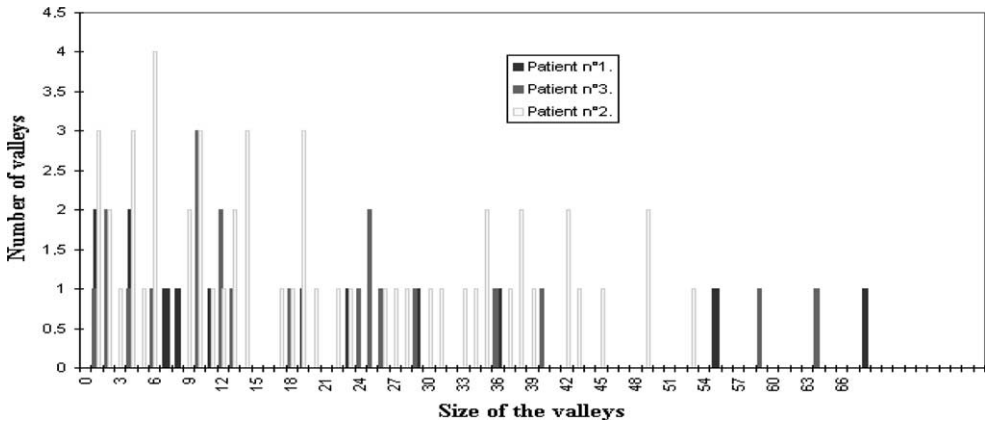

Fig. 8. Histogram of the valley sizes.

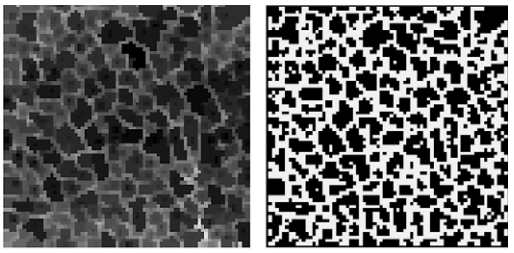

Fig. 9. Results of the thinning and of the crest line from a 4 bits coded dynamics.

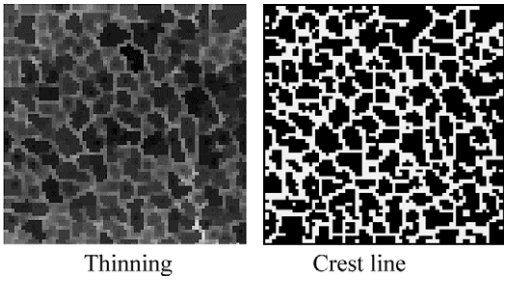

Fig. 10. Results of the thinning and of the crest line from a 8 bits coded dynamics.

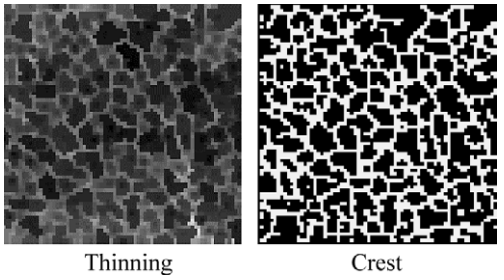

Fig. 11. Results of the thinning and of the crest line from a 12 bits coded dynamics.

the computed parameters. We therefore calculated the previously defined parameters from the different dynamics for controls patients (15 healthy women before menopause) and patients after menopausal (7 menopausal women and 8 menopausal osteoporotic women). The results are given in Table 2.

We can observe that, whatever the dynamics used, the five features calculated have not the same discrimination power. Actually, the ranges of variations are more important for the parameters crest length and the average size of the large valleys.

Moreover, these two parameters seem to be the most significant ones for characterizing the trabecular bone, as bone frameworks are represented by the crests and the space between bone frameworks is represented by the large valleys. In addition, the table reveals that the range of variation of these five features decreases with the increase of the gray-levels dynamics.

This remark is all the more true for the two previously quoted parameters. Indeed, for the parameter of the crest length, we obtain values ranging in the interval $[30.96, 39.04]$ with the 4 bits coded dynamics and in the interval $[48.98, 49.19]$ with the 12 bits dynamics. In the same way, for the average size of the large valleys we get a range of value $[43.64, 61.76]$ with the 4 bits coded dynamics and $[25.62, 27.18]$ with the 12 bits coded dynamics. From these results, we notice that the discrimination will be better if we use a 4 bits coded dynamics because of these larger ranges.

In this preliminary study, though limited to 30 patients, we have seen that by using a weak dynamics of gray-level, we obtained a more important range of the measured parameters. This is why we finally opted for a dynamics restricted to 4 bits coding. Furthermore, the average size and the total number of small valleys will not allow a good discrimination, considering their little range of variations. In these circumstances, we can suppress the parameters exclusively calculated from small valleys. Nevertheless, this study is a preliminary one and the population under testing is to increase, we will preserve some information on the small valleys so as to check their influence. Then we define a parameter gathering the small and the large valleys: the average size of all valleys. Consequently, the retained attributes are: the crest length, the number of valleys (both referred to the size of the ROI), the average size of the large valleys and the average size of all the valleys.

We also noted that the results obtained in terms of discrimination between the two groups (II and III) are better on coronal than on axial slices. In fact, for the parameter of the crest length, we ob-

Table 2
Values (mean ± standard deviation) of the computed parameters from coronal slices

	Control patients ($n = 15$)	Menopausal women ($n = 7$)	Menopausal osteoporotic women ($n = 8$)
Crest length/ROI size (in %)			
4 bits dynamics	39.04 ± 1.5 ($p < 0.03$)	35.3 ± 2.5 ($p < 0.03$)	30.96 ± 2.0 ($p < 0.03$)
8 bits dynamics	44.5 ± 2.05	38.59 ± 4.8	41.88 ± 1.55
12 bits dynamics	49.19 ± 3.8	46.48 ± 3.5	48.98 ± 2.85
Average size of the large valleys/ROI			
4 bits dynamics	43.64 ± 3.05 ($p < 0.03$)	57.53 ± 1.95 ($p < 0.03$)	61.76 ± 2.25 ($p < 0.03$)
8 bits dynamics	32.22 ± 5.05	38.67 ± 4.65	35.2 ± 3.75
12 bits dynamics	25.62 ± 2.15	25.61 ± 3.5	27.18 ± 3.35
Number of large valleys/ROI size (in %)			
4 bits dynamics	1.39 ± 0.5 ($p < 0.04$)	1.12 ± 0.1 ($p < 0.04$)	1.12 ± 0.17 ($p < 0.04$)
8 bits dynamics	1.69 ± 0.2	1.58 ± 0.8	1.64 ± 0.6
12 bits dynamics	1.92 ± 0.25	2.04 ± 0.55	1.84 ± 0.35
Average size of the small valleys/ROI			
4 bits dynamics	1.83 ± 0.13 ($p < 0.05$)	3 ± 0.11 ($p < 0.05$)	0
8 bits dynamics	2.33 ± 0.35	1.2 ± 0.25	2 ± 0.17
12 bits dynamics	2.13 ± 0.3	1.82 ± 0.5	2.14 ± 0.13
Number of small valleys/ROI size (in %)			
4 bits dynamics	0.2 ± 0.01 ($p < 0.05$)	0.13 ± 0.02 ($p < 0.05$)	0
8 bits dynamics	0.5 ± 0.1	0.33 ± 0.89	0.13 ± 0.012
12 bits dynamics	0.79 ± 0.025	0.72 ± 0.05	0.46 ± 0.03

tained values ranging in the interval $[34.56, 36.14]$ with the 4 bits coded dynamics and in the interval $[49.08, 49.23]$ with the 12 bits dynamics. In the same way, for the average size of the large valleys we get a range of value $[55.24, 62.06]$ with the 4 bits coded dynamics and $[26.34, 27.91]$ with the 12 bits coded dynamics We think that this finding might be due to the anisotropy of the radius, which is possibly more pronounced in osteoporotic patients than in controls.

6. Conclusion

We developed original methods for the analysis and the characterization of the bone texture. These methods are based on the numerical processing of CT-scan images. Our results suggest that bone texture analysis might be a useful tool in the assessment of osteoporosis. However, not all the methods presented and all the features measured were equally useful in terms of discriminating between osteoporotic women and controls.

In summary, firstly, results of our work, a priori and a posteriori, show that fractal analysis seems effective notably in terms of discrimination between osteoporosis women and controls.

The most promising structure parameters for CT images are fractal dimension, fractal signature, for fractal analysis (i.e., by using the method of morphological covers).

Secondly, the most promising structure parameters for CT images are the crest length, the number of valleys (both referred to the size of the ROI), the average size of the large valleys and the average size of all valleys, for the structural approach. We have seen that by using a weak dynamics of gray-level, we obtained a more important range of the measured parameters (i.e., for a dynamics restricted to 4 bits coding). In the future, we must verify and take into account the reproducibility of the features used for the characterizing of bone texture.

In conclusion, this preliminary study advocates interest in CT-scan analysis of the distal radius in detecting osteoporosis related changes in trabecular

bone texture. These changes are in harmony with those found in histo-morphometric studies (Croucher and Compston, 1996).

Acknowledgement

The authors would like to thank J.M. Folzan for his advice.

References

Benhamou, C.L., Harba, R., 1994. Changes in fractal dimension of trabecular bone in osteoporosis: a preliminary study. Birkaüser Verlag, pp. 292–299.

Benhamou, C.L., Lespessailles, E., 1994. Fractal organization bone images on calcaneus radiographs. J. Bone Miner. Res. 9 (12), 98–105.

Buckland-Wright, J.C., Lynch, J.A., 1994. Fractal signature analysis of macroradiographs measures trabecular organization in lumbar vertebrae of postmenopausal women. Calcif. Tissue Int. 54, 106–112.

Cortet, B., Dubois, P., 1998. Image analysis of the distal radius trabecular network using computing tomography. Osteoporis Int. 9 (4), 410–419.

Cortet, B. et al., 2000. In vivo comparison between CT and MR image analysis of the distal radius in the assessment of osteoporosis. J. Clini. Dens. 3, 15–26.

Croucher, P.I., Compston, J.E., 1996. Assessment of cancellous bone structure: comparison of structure analysis trabecular bone pattern factor and narrow space star volume. J. Bone Miner. Res. 7, 955–961.

Cuisenaire, O., 1999. Fast Euclidean morphological operators using local distance transformation by propagation. Internat. Symp. Pattern Recog., Brussels, 1999.

Hausdorff, F., 1919. Dimension und ausseres mass. Mathe. Annatlen 79, 157–179.

Jin, X.C., Ong, S.H., 1995. A practical method for estimating fractal dimension. Patt. Recogn. Lett. 6, 457–464.

Lespessilles, E., Eynard, E., 1996. Effects of age and menopause on fractal dimension of trabecular bone determined on calcaneus radiographs. J. Bone Miner. Res. 11, 473–478.

Lynch, J.A., Hawkes, D.J., 1991. Analysis of texture in macroradiographic of osteoarthritic knees using the fractal. signature. Phys. Med. Bio. 36, 709–722.

Majunbar, S., Link, T., 1999. Trabecular bone architecture in the distal radius using MR imaging in subjects with fractures of proximal femur. J. Radio. 10, 231–239.

Majunbar, S., Genant, H.K., 1997. Correlation of trabecular bone structure with age in vivo studies in distal radius using high resolution MRI. J. Bone Miner. Res. 12, 111–118.

Mandelbrot, B., 1975. In: Flammarion (Ed.), Les objets fractals: Forme, hasard, dimension, paris.

Minkowski, H., 1901. Uber die begriffe lange, Ober flache und Volumen, Jahresbericht der Deutschen Mathe. Vereinigung, Vol. 9, pp. 115–179, 1901.

Muller, R., Hahn, M., 1996. Morphometric analysis of noninvasively assessed bone biopsies: Comparison of high resolution computed tomography and histologic section. J. Bone Miner. Res. 18, 1745–1751.

Osman, D., Newitt, D., 1998. Fractal based image analysis of human trabecular bone using the BC algorithm. World Scientific Publis. Comp. Fractal. 6 (3), 275–283.

Peleg, S., 1984. Multiple resolution texture analysis and classification. IEEE Trans. PAMI 6, 661–674.

Pothuaurd, L., Lespessailles, E., 1998. Fractal analysis of trabecular bone texture on radiographs: discriminant value in postmenopausal osteoporosis. Adv. Osteoporose Bone quality 8, 618–625.

Prasad, R., Majunbar, S., 1991. Fractal geometry as a means of studying trabecular bone structure. Nuclear Science Symp. And medical imaging conf., 1844–1848.

Saupe, D., 1988. Algorithms for Random Fractals in the Science of Fractal Images. Springer Verlag, pp. 71–133.

Serra, J., 1982. Image Analysis and Mathematical Morphology. Edt Press-London.

Taleb-Ahmed, A., Dubois, P., Duquemoy, E., 2000. A new method for bone texture analysis and characterization, IEEE IWISPA, pp. 163–168, Paula Croatia.

Vieth, D., 2000. Comparison of Trabecular Bone Structure Measured in Macro-Pathological Sections and High Resolution (HR) MR Images, 14th Inter. Bone Densitometry Workshop, pp. 3–8.